

In “Sediment and Ecohydraulics: INTERCOH 2005”. T Kusuda, H Yamanishi, J Spearman and J.Z Gailani (Editors)

2008 ; Proceedings in Marine Science 9, Pages 431-446  
© 2008 Elsevier B.V. All rights reserved.

Archimer  
Archive Institutionnelle de l'Ifremer  
<http://www.ifremer.fr/docelec/>

---

## Sedimentary processes in a shellfish farming environment, Mont Saint Michel Bay, France

Cayocca F.<sup>1,\*</sup>, Bassoullet P.<sup>1</sup>, Le Hir P.<sup>1</sup>, Jestin H.<sup>1</sup>, Cann P.<sup>1</sup>

<sup>1</sup> IFREMER, Département DYNECO, Laboratoire PHYSED, B.P. 70, 29280 Plouzané, France

\*: Corresponding author : Cayocca F., email address : [Florence.Cayocca@ifremer.fr](mailto:Florence.Cayocca@ifremer.fr)

---

### Abstract:

Mont Saint Michel Bay is a 30 km wide bay located on the French side of the English Channel. The tidal range reaches 14 m during spring tides, which leads, along with the gentle slope of the bathymetry, to a tidal flat up to 11 km wide. The sedimentary coverage exhibits strong longshore and cross-shore gradients, with purely muddy environments to the west of the domain, and pure sands to the east, where the natural channels of three incoming rivers induce rapid morphological changes. The contributions of tides and waves to sedimentary processes are analysed by means of numerical modelling and results of field observations. Maximum tidal bottom shear stresses are shown to account for the sediment distribution throughout the bay, while the longshore gradient in wave intensity seems to drive the amount of suspended sediment concentration. The bay has been a privileged ground for shellfish farming for over a century. Farming structures (oyster tables, mussel posts and wooden fences used as permanent fishing nets) have significantly hindered natural flow patterns, creating quiescent areas which significantly increase fine sediments deposits in farming areas. The paper focuses on introducing into a numerical model the effects of mussel farms on flow circulation and sediment dynamics.

---

## 1. INTRODUCTION

Mont Saint Michel Bay lies on the French coast of the English Channel in a macrotidal environment (one of the world's largest tidal ranges, up to 14 m during spring tides). The bay is one of the largest farming grounds for oysters and mussels on the French side of the English Channel. Since shellfish production has significantly decreased in the past 10 years, assessing the trophic capacity of the bay (i.e. the availability of food for raised and native species) has become an ecological priority while, at the same time, the restructuring of shellfish farming is required to counteract the unmanageable mud deposits encountered in oyster beds. These ecological as well as economical concerns are related to turbidity levels (which affect plankton growth as well as shellfish ecophysiology) and sediment transfers in the bay (which affect the native benthic population and also lead to mud deposits around farming structures). As part of a multidisciplinary project, a major hydrodynamic and sedimentological study was initiated in 2001 to describe the local conditions and explain the physical processes driving sediment transfers.

## 2. CONTEXT AND SETTING

Freshwater input to the Mont Saint Michel Bay arrives principally from its southwest corner where three small rivers of fairly limited discharge (average discharge on the order of 25 m<sup>3</sup>/s) compared to the volume of the bay (tidal prism of 2300 Mm<sup>3</sup> for a mean tide and 2000 Mm<sup>3</sup> for low tide, see Fig. 1) feed the bay. The bay is characterized by a 4 km wide tidal flat in its central area (up to 11 km in the east) with a 1/550 slope. Maximum tidal current velocities vary from 0.4 m/s on the tidal flats to 1 m/s at the northern limit of the bay, with local maxima encountered in the channels and by the cape to the north-west of the domain. The largest waves come from propagation in the Atlantic Ocean; offshore wave heights are greater than 0.8 m and smaller than 2 m for 50% of the time.

AQ1

The bay has undergone continuous infill in the past centuries, as illustrated by the seaward progression of lowlands now used for agriculture. This feature results from the flood dominance of the tide and illustrates what Le Hir et al. (2005) called intrinsic asymmetry (i.e. deposition on the upper flat during high water slack, followed by partial consolidation which does not allow erosion to occur during the ebb) and large-scale asymmetry (non-linear distortion of the tide during propagation). The present rate of infill has been estimated to be 0.2 cm/year on average (Migniot, 1998).

AQ2

Several man-made structures were introduced into the environment, above the level of lowest low tide (Bahé, 2003), namely fish traps, oyster tables and mussel farms, all of

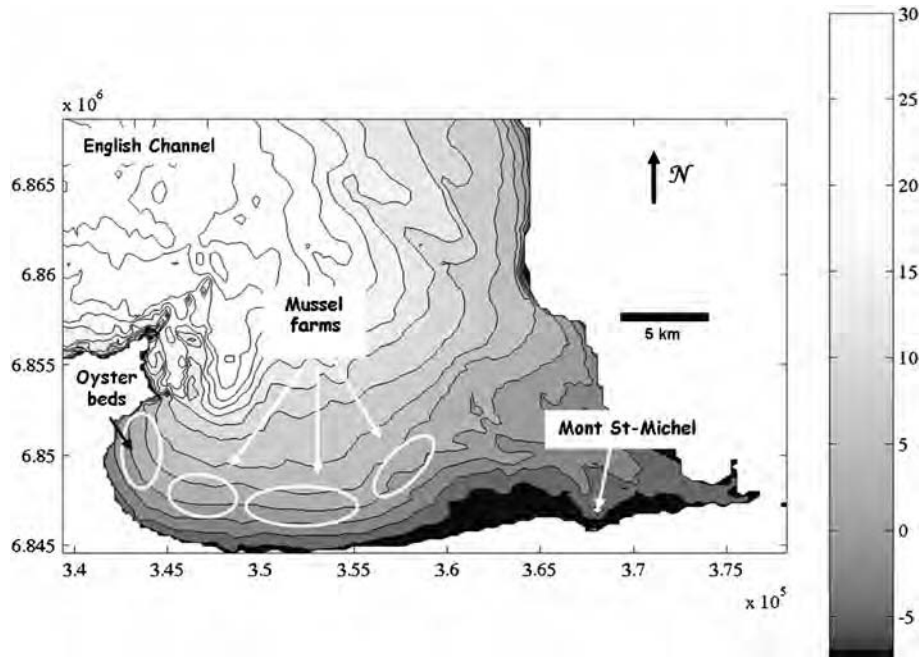


Figure 1. General setting of Mont Saint Michel Bay. Water depths are relative to the level of the lowest low tide. Isolines every 2.5 m.

1b which have considerably modified the sediment distribution in the bay. We will focus here  
2 on the mussel farms, which were installed in the central part of the bay in the 1960s. They  
3 consist of rows of 2.4-m-tall posts around which lines of mussel spawn are rolled spirally.  
4 The posts eventually grow to 70 cm in diameter. They lie in the centre of the bay in a fine  
5 sand environment and experience very local temporary mud deposits at their bases.

6 Increased sedimentation around farming structures is detrimental to shellfish growth.  
7 Moving the farms is often found as the only short-term solution when shellfish production  
8 decreases to an unacceptable level. However, up to now, no numerical tool was capable of  
9 predicting long-term morphodynamic evolutions of such environments, where the sedi-  
10 ment behaviour is further modified by the presence of bio-deposits.

11 This work is a first step towards understanding processes responsible for the natural and  
12 man-made infill of the bay by means of numerical modelling. The main simplifications  
13 applied here are that wave action is not included in the model and only a single mud frac-  
14 tion is represented.

15

16

### 17 **3. OVERVIEW OF THE MAIN HYDRODYNAMIC AND SEDIMENTARY** 18 **PROCESSES FROM A NUMERICAL MODEL AND DATA**

19

20 A 2D finite difference model, SiAM2D, was used to solve the shallow-water equations on  
21 an irregular Cartesian grid. This 2D approach was justified by the small freshwater inputs  
22 as well as the intense vertical mixing due to strong tidal currents.

23 Computed water levels and current velocities were validated against three sets of tidal  
24 gages as well as results from a SAMPLE monitoring station (Jestin et al., 1994) deployed  
25 on the tidal flat in 2003 and 2004. Currents were measured 0.3 m above the sea floor with  
26 an electromagnetic current meter, turbidity was recorded with two OBS sensors at 0.1  
27 and 0.3 m above the sea floor, and water height was measured with a pressure sensor. In  
28 order to compare vertically integrated computed velocities with local measurements, a  
29 logarithmic velocity profile was assumed. An equivalent vertically integrated ‘measured’  
30 velocity was therefore used for comparisons with model outputs. The roughness length  
31 was computed from the ripple characteristics ( $z_0 = 0.002$  m). Fig. 2 shows the measured  
32 and computed velocity components and water heights for a mean tide in the central part  
33 of the bay. The variation in water level is reasonably well reproduced for neap tides, and  
34 very well reproduced for spring tides. A systematic phase shift of 20 min had to be  
35 applied to the boundary conditions in order to obtain this result (tidal harmonics com-  
36 puted from the French Naval Research, Le Roy and Simon, 2003). Recorded velocities  
37 are only valid when the current meter is immersed, i.e. when the water height exceeds  
38 0.3 m. Eastward velocities are sometimes slightly over-predicted; however, judging by  
39 the small magnitude of this component, model results are considered very reasonable.  
40 The maximum magnitude of the northward component is very well reproduced. The  
41 modelled velocity rapidly reaches a maximum during the flood and remains constant at  
42 its maximum value for over 2 h. This could be due to an underestimation of the friction  
43 for larger water heights (the friction was computed with a uniform Strickler coefficient  
44 of  $45 \text{ m}^{1/3}/\text{s}$ , except in the westernmost part of the bay where the friction was enhanced in  
45 order to account for the presence of oyster tables). When maximum velocities exceed an  
46 erosion threshold, we can expect to overestimate the time during which erosion occurs.

AQ3

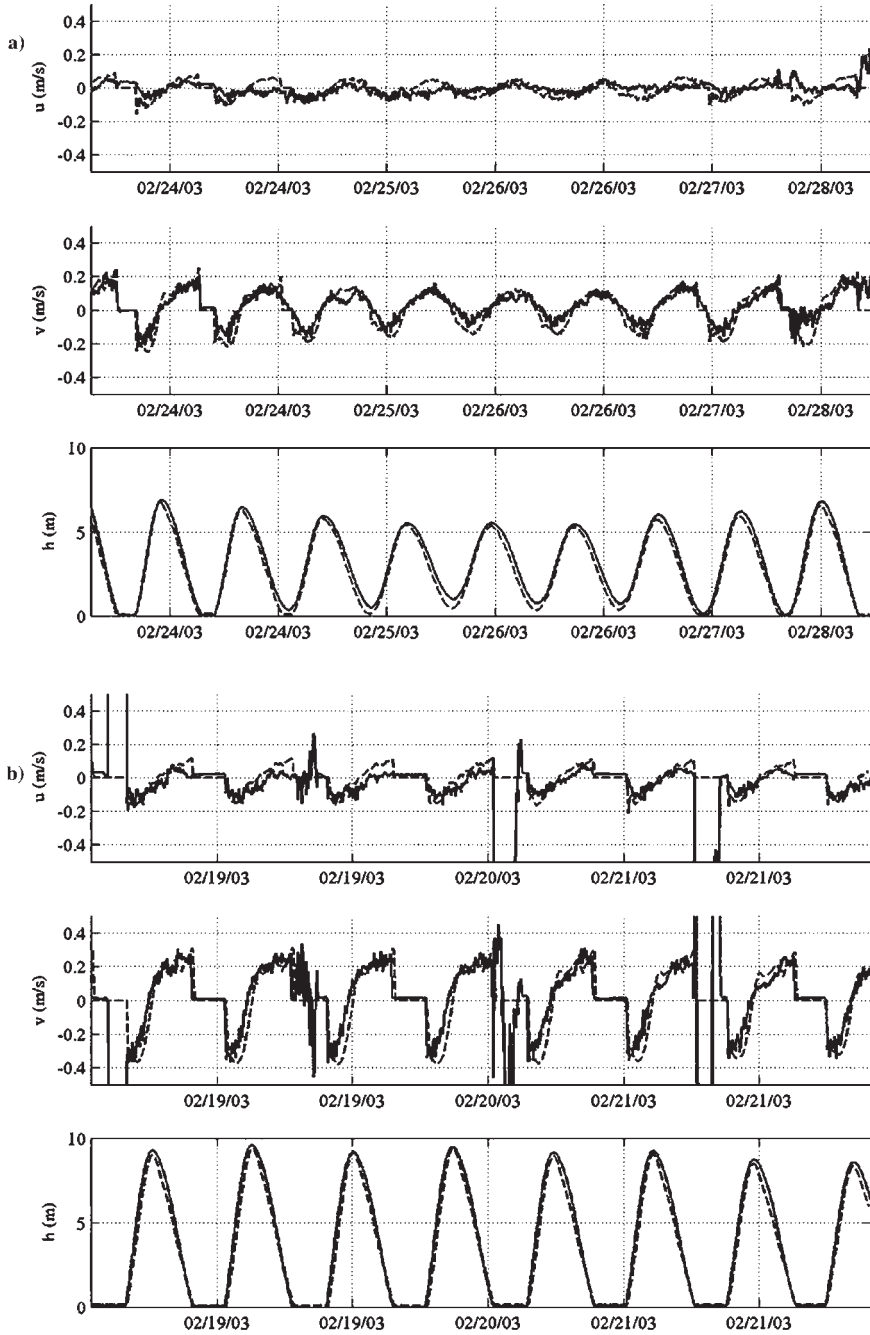


Figure 2. Comparison between model results (dashed line) and measurement (solid line) on the tidal flat (a) during neap tide and (b) during spring tide; on each graph, from top to bottom: east–west velocity (positive eastwards), north–south velocity (positive northwards) and water height.

1b  
2  
3  
4  
5  
6  
7  
8  
9  
10  
11  
12  
13  
14  
15  
16  
17  
18  
19  
20  
21  
22  
23  
24  
25  
26  
27  
28  
29  
30  
31  
32  
33  
34  
35  
36  
37  
38  
39  
40  
41  
42  
43  
44  
45  
46

1b  
2  
3  
4  
5  
6  
7  
8  
9  
10  
11  
12  
13  
14  
15  
16  
17  
18  
19  
20  
21  
22  
23  
24  
25  
26  
27  
28  
29  
30  
31  
32  
33  
34  
35  
36  
37  
38  
39  
40  
41  
42  
43  
44  
45  
46

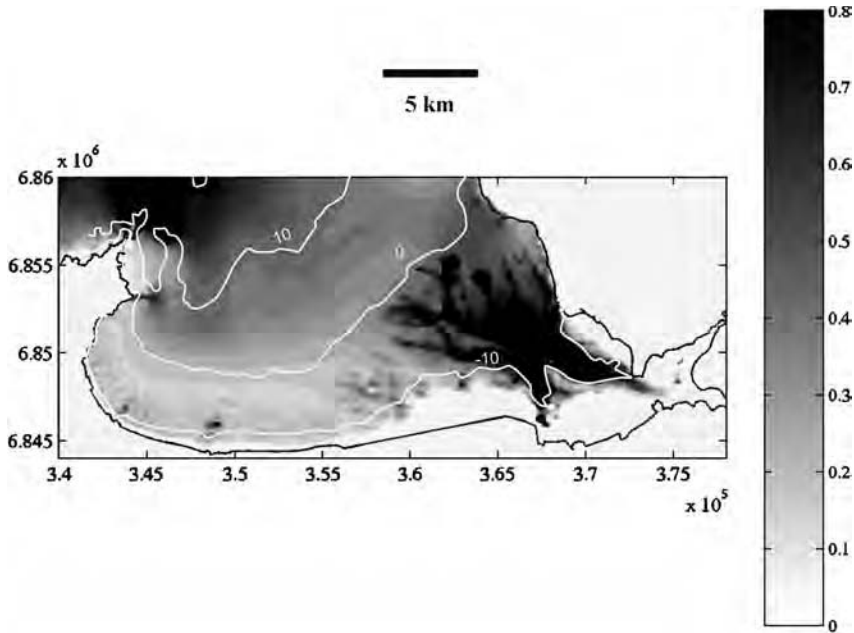


Figure 3. Magnitude of the maximum tidal current velocities in m/s for a mean spring tide. The thin white lines show the -10, 0 and 10 m isobaths, the datum being the level of low tide for extreme spring tides.

The transport of cohesive sediments is computed by solving an advection–diffusion equation in the water column, where deposition and erosion fluxes constitute the sediment source and sink terms (Le Hir et al., 2005). Hindered settling is taken into account by prescribing a relationship between the settling velocity and the suspended concentration (see Section 5).

Fig. 3 shows the maximum velocity field for a mean spring tide. Large values are encountered by the north-west cape of the bay as well as by the channels found in the eastern part of the bay. The lowest velocities occur in the central and western areas of the domain (apart from very local higher values where small rivers feed the system). This longshore trend in the maximum velocity field reinforces longshore effects due to the wave propagation pattern. In the cross-shore direction, maximum velocities decrease shoreward, before increasing again where the bathymetry exceeds MSL of 2 m. The maximum velocity decreases again on the higher flat. Such velocity increase is not observed in the westernmost part of the bay.

These features are in good agreement with the sediment distribution as depicted in Fig. 4: muddy sediments are encountered all around the bay on the higher part of the tidal flat (typically above MSL of +4m), and all the way down to MSL. However, in the central part of the bay, muddy sands are found along a strip that roughly corresponds to the area of higher maximum tidal velocities. Pure sand is found where mean spring tide velocities exceed 0.5 m/s.

Waves, water levels and concentration of suspended particulate matter were monitored at several sites over several months, 20 cm above the bottom. Fig. 5 shows results in two

1b  
2  
3  
4  
5  
6  
7  
8  
9  
10  
11  
12  
13  
14  
15  
16  
17  
18  
19  
20  
21  
22  
23  
24  
25  
26  
27  
28  
29  
30  
31  
32  
33  
34  
35  
36  
37  
38  
39  
40  
41  
42  
43  
44  
45  
46

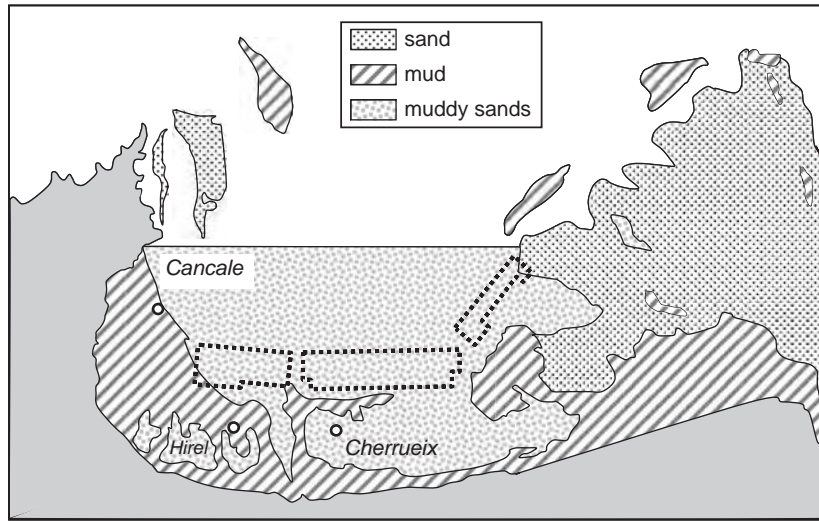


Figure 4. Simplified sediment distribution in the Mont Saint Michel Bay (modified from Ehrhold, 1999). 'Cancale', 'Hirel' and 'Cherrueix' are the names of the monitoring stations described in the text. Dotted lines represent the mussel farms contours. **AQ7**

of these monitoring stations. The westernmost monitoring station ('Cancale', see Fig. 4 for location) was located at the edge of the lowest spring tide level, in purely muddy environments. The pattern of suspended matter concentration follows very well the tidal fortnightly cycle, with sharp peaks at the beginning of the flood and at the end of the ebb. A given offshore wave condition necessarily induces higher waves at a given location during spring tides than during neap tides, since the water level is higher; this explains why higher waves are generally measured during spring tides. However, concentrations are not strongly correlated with waves.

The monitoring station of the central part of the bay ('Cherrueix') was located in sandy environments. The fortnightly cycle does not influence suspended matter concentrations there, which are, on the other hand, related to incoming waves. Concentration results at an intermediary location ('Hirel', sandy muds, plot not shown) exhibit intermediary features, where the influence of both tides and waves can be seen.

The wave propagation pattern in the bay shows smaller waves in the western part, where incoming waves (mostly from the north-west region outside the bay) have been diffracted by the northwestern cape. This pattern, along with modelling and monitoring results, suggest the following:

- tidal dynamics accounts for a large part of the sediment distribution in the bay, since maximum tidal bottom shear stresses are well correlated with the sediment coverage;
- resuspension events are related to the action of both tides and waves. In the central part of the bay, waves dominate over the tides and are responsible for the main part of the suspended matter. This trend reverses as we move west, where the effect of the waves is progressively dampened in favour of a mostly tidal effect.



1b  
2  
3  
4  
5  
6  
7  
8  
9  
10  
11  
12  
13  
14  
15  
16  
17  
18  
19  
20  
21  
22  
23  
24  
25  
26  
27  
28  
29  
30  
31  
32  
33  
34  
35  
36  
37  
38  
39  
40  
41  
42  
43  
44  
45  
46

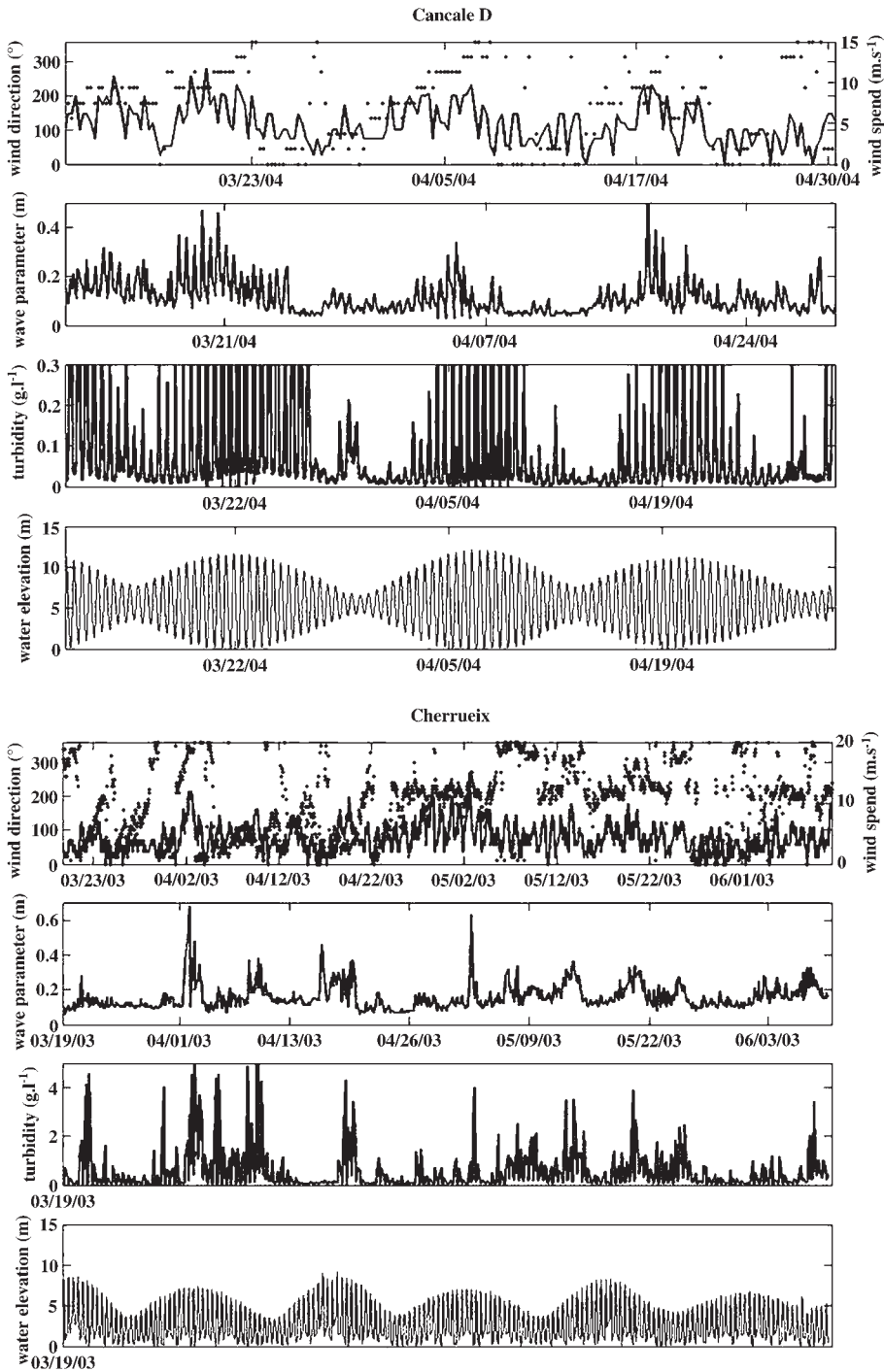


Figure 5. For the western part of the bay (upper graph, Cancalle) and the central part of the bay (bottom graph, Cherruex), time series of the wind (speed in bold line, direction in dots), wave height, turbidity and water level.

#### 4. MODEL REPRESENTATION OF MUSSEL FARMS

Very few studies have investigated the effects of mussel farms on flow. Recently, SEAMER (2000) used a numerical model with a 10-cm mesh to compute the hydrodynamic effects of 2.4 m tall posts 0.4 m in diameter, representing average-size mussel posts ('empty' posts are 0.2 m in diameter; they can be as large as 0.7 m in diameter when covered with mature mussels). For a single post, the current velocity was shown to increase on both sides of the post as long as it emerged, while the velocity decreased upstream of the post as well as in the downstream wake. The wake of an individual post where the velocity was decreased by 80% was a few metres long, depending on the ambient velocity and water height. A row of such posts aligned with the current direction induced a 10% velocity decrease over 1–2 m on both sides of the row. When the current direction was not aligned with the row, the width of the wake increased significantly, and the overall velocity could decrease by up to 30%. However, a row of posts covered by 1 m of water induced very local accelerations and decelerations of the flow, but had no influence on the overall current velocity (which was probably due to the fact that velocities were vertically integrated). Unfortunately, these simulations were only carried out for fairly restrictive conditions (current velocity of 1 m/s, one single diameter, three water heights), were not validated against data and did not allow for a general parameterization of the effects of the posts on the flow.

SOGREAH (1986) carried out physical experiments in order to quantify the overall slowing down of the flow expressed through a variable Strickler coefficient. This coefficient was shown to vary from 18 to 32 depending on the distance between posts and between rows, the size of the posts, the incidence of the current compared to the posts and the reference Strickler coefficient of a domain without mussel farms. The orientation of the tidal ellipses in the Mont Saint Michel Bay follows bathymetric gradients, whereas rows of mussel posts are oriented north-south in the whole western and central farming areas, and oriented north-west–south-east in the eastern farming area. This disposition was chosen to minimize impacts on the tidal propagation; however, the angle between the rows and the tidal current varies throughout the bay. As a first approach, we considered a constant and uniform Strickler coefficient of  $25 \text{ m}^{1/3}/\text{s}$  in the farming areas, which is representative of an average post dimension (*cf.* SOGREAH for more details).

Fig. 6 shows the maximum effect of the farms on current velocities during the flood and during the ebb, for a spring tide. The maximum effect is observed within the farms (deceleration) and on the eastern and western ends of the farms (acceleration of the flow that goes around the areas of increased friction); these effects are felt several kilometres away from the farm. Fig. 7 gives a quantitative estimate of the velocity changes for a mean tide. Similar patterns are actually observed for spring tides, i.e. acceleration of up to 30% on the edge of the farms (point A), deceleration of 5% up to 2 km north of the farms (point E) and deceleration of 10% within the farms (point F). These differences are likely to substantially modify deposition and erosion patterns.

#### 5. SEDIMENT TRANSFERS

Our ultimate goal is to assess the effect of mussel farms on long-term sedimentation. The discussion presented in Section 3 indicates that we may consider that the tidal current



1b  
2  
3  
4  
5  
6  
7  
8  
9  
10  
11  
12  
13  
14  
15  
16  
17  
18  
19  
20  
21  
22  
23  
24  
25  
26  
27  
28  
29  
30  
31  
32  
33  
34  
35  
36  
37  
38  
39  
40  
41  
42  
43  
44  
45  
46

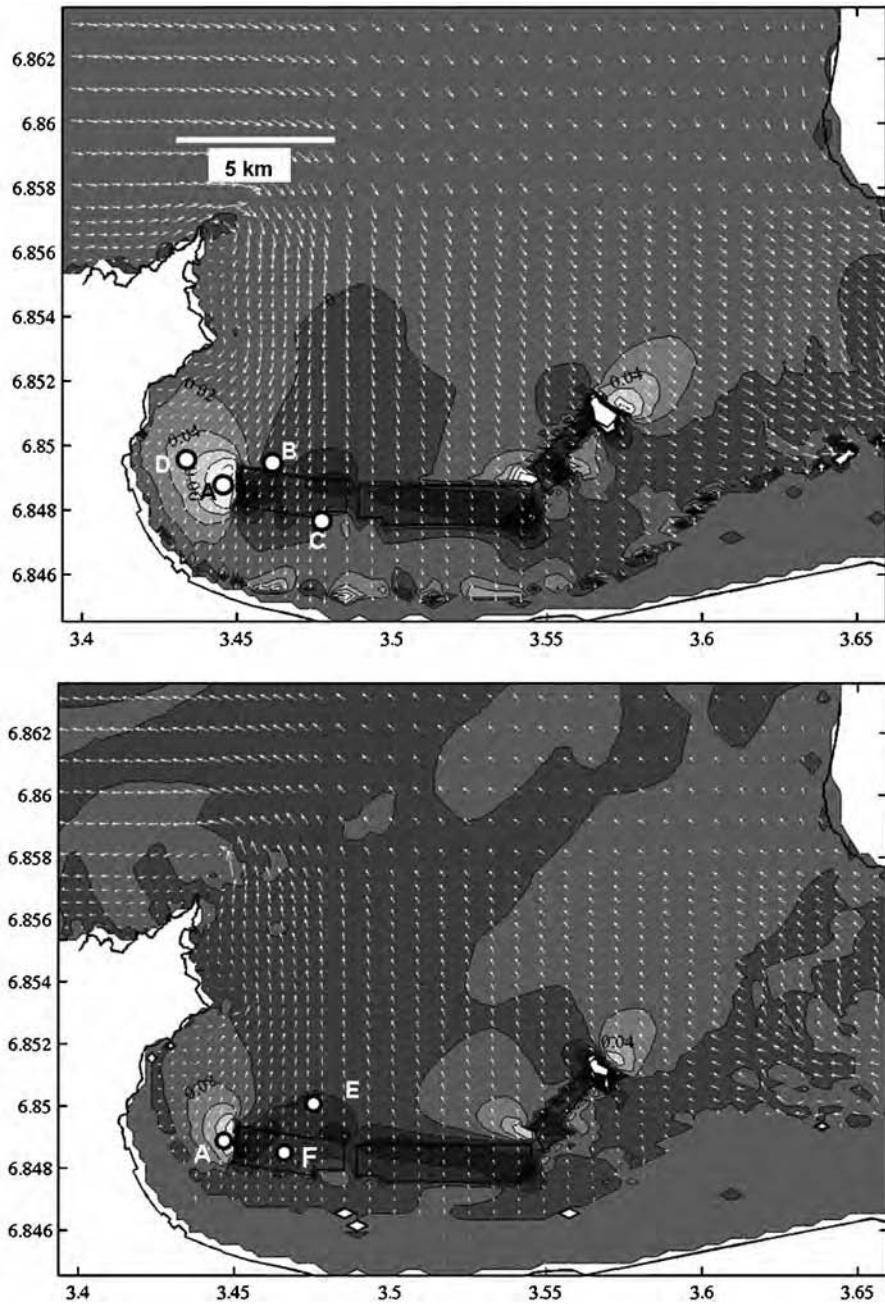


Figure 6. Contours of velocity differences between a situation with farms and a situation with no farms during the flood (top) and the ebb (bottom) (in metres). Isolines every 0.02 m/s. Spring tide. Lighter shades represent a velocity increase, darker shades a velocity decrease.

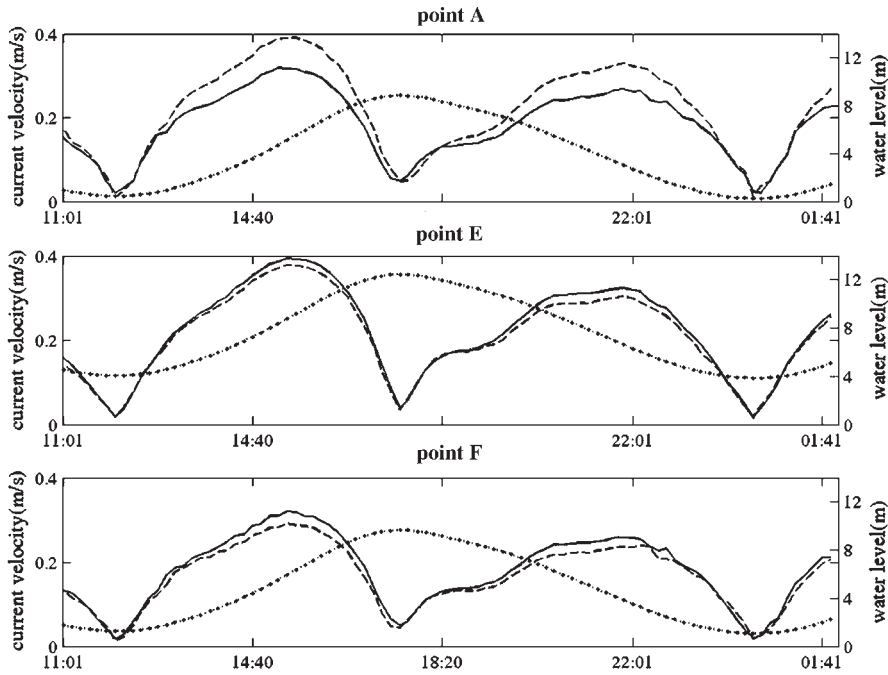


Figure 7. Water height (dots) and magnitude of the current velocity with (solid line) or without (dotted line) mussel farms. Top: point A, centre: point E, bottom: point F.

largely accounts for the sediment distribution. We therefore restrict the study to a situation where only tides are taken into account and waves are disregarded. Considering a single mud fraction, our strategy consists in comparing mud sedimentation patterns with or without mussel farms, from an initially uniform sedimentary coverage.

Results without farms must first be compared to field observations. The model is first run for the year 2003, considering an initial uniform fine sediment coverage of 0.3 m throughout most of the domain (the exact contour of the covered area actually follows the limit of zones where a significant mud content was identified on the map of sediment coverage). Hydraulic roughness used for velocity computations is represented by a Strickler friction coefficient of  $45 \text{ m}^{1/3}/\text{s}$ . On the other hand, the bottom shear stress that drives the sediment erosion is computed from a Nikuradse roughness ( $z_0 = 0.0002 \text{ m}$ ). This roughness is assumed to be uniform and constant throughout the runs. The initial bottom concentration is taken to be  $800 \text{ kg/m}^3$ , which corresponds to a typical concentration measured in the field.

Erosion is parameterized according to Partheniades' law:

$$E = E_0 \frac{\tau - \tau_{cr}}{\tau_{cr}} \text{ [kg/m}^2/\text{s]} \quad (1)$$

where  $\tau$  is the bottom shear stress. The erosion threshold  $\tau_{cr}$  (expressed in  $\text{N/m}^2$ ) depends on the sediment concentration in the sediment surface layer  $c_s$  (expressed in  $\text{kg/m}^3$ ).

1b Laboratory experiments were carried out by Migniot (1998) in order to assess the relationship  
 2 between  $\tau_{cr}$  and  $c_s$ . Migniot's results were fitted with a bilinear relationship:

$$3 \quad \tau_{cr} = \alpha_1 c_s \quad \alpha_1 = 0.0002 \text{ m}^2/\text{s}^2 \quad \text{for } c_s < 500 \text{ kg/m}^3 \quad (2)$$

$$4 \quad \tau_{cr} = \alpha_2 c_s + \beta_2 \quad \alpha_2 = 0.0014 \text{ m}^2/\text{s}^2 \quad \beta_2 = -0.6 \text{ N/m}^2 \quad \text{for } c_s \geq 500 \text{ kg/m}^3 \quad (3)$$

5  
6 This relationship leads to critical shear stresses of about 0.5 N/m<sup>2</sup> for the concentration  
7 of a surface sediment of 800 kg/m<sup>3</sup> (consolidated) and of about 0.03 N/m<sup>2</sup> for a fresh  
8 deposit (150 kg/m<sup>3</sup>).

9 Erosion tests carried out in a flume on sediment cores sampled in the field showed that  
10 for silt and clay mixtures encountered in the western part of the bay,  $E_0$  ranged from  
11 0.0001 to 0.0003 kg/m<sup>2</sup>/s (Le Hir et al., 2006). Results shown here were computed with  
12  $E_0 = 0.00015 \text{ kg/m}^2/\text{s}$ .

13 The eroded sediment is advected in the water column and settles at the settling velocity  
14  $w_s$ , which is parameterized as a function of the sediment concentration (hindered settling).  
15 The settling velocity was not measured in the study area; we therefore use parameters in the  
16 range found in the literature. Here,  $w_s$  increases from 0.15 to 1.5 mm/s for concentrations  
17 ranging from 1 to 100 g/L and then decreases ( $w_s = 0.15 \text{ mm/s}$  for a concentration of  
18 450 g/L). Deposition fluxes are computed according to the following equations:

$$19 \quad D_{\text{flux}} = w_s \cdot c_w \cdot \frac{\tau_{\text{crdep}} - \tau}{\tau_{\text{crdep}}} \quad \text{if } \tau < \tau_{\text{crdep}} \quad (4)$$

$$20 \quad D_{\text{flux}} = 0 \quad \text{if } \tau > \tau_{\text{crdep}}, \quad (5)$$

21 where  $c_w$  is the sediment concentration in the water column and  $\tau_{\text{crdep}}$  a critical deposition  
22 shear stress above which the turbulence level is too high for deposition to occur. Since erosion  
23 and deposition occur simultaneously in nature,  $\tau_{\text{crdep}}$  is set to a very high value (10 N/m<sup>2</sup>),  
24 so as to allow deposition most of the time, in which case the sediment is immediately  
25 eroded again if the shear stress exceeds the critical erosion shear stress. Deposited sedi-  
26 ment is otherwise prescribed a 'fresh deposit' concentration of 150 g/L. Depending on the  
27 bottom concentration, fresh deposits may merge with the existing sediment (and thereafter  
28 consolidate), or be considered as a low-concentration layer that will be allowed to consol-  
29 idate independently from the underlying layer.

30 Consolidation is taken into account in the sediment compartment, where we solve

$$31 \quad \frac{\partial c}{\partial t} + w_{\text{sed}}(c) \frac{\partial c}{\partial z} = 0 \quad (6)$$

32 where  $w_{\text{sed}}$  is a sedimentation velocity in the sediment, parameterized as a function of the  
33 porosity. In this case, this function has been adjusted so as to reproduce experimental  
34 results of settling columns described by Migniot (1998). An important feature of the  
35 muddy sediments encountered in the bay is their high calcareous content, which induces  
36 exceptionally high compaction rates. Fig. 8 shows the computed evolution of the height

1b  
2  
3  
4  
5  
6  
7  
8  
9  
10  
11  
12  
13  
14  
15  
16  
17  
18  
19  
20  
21  
22  
23  
24  
25  
26  
27  
28  
29  
30  
31  
32  
33  
34  
35  
36  
37  
38  
39  
40  
41  
42  
43  
44  
45  
46

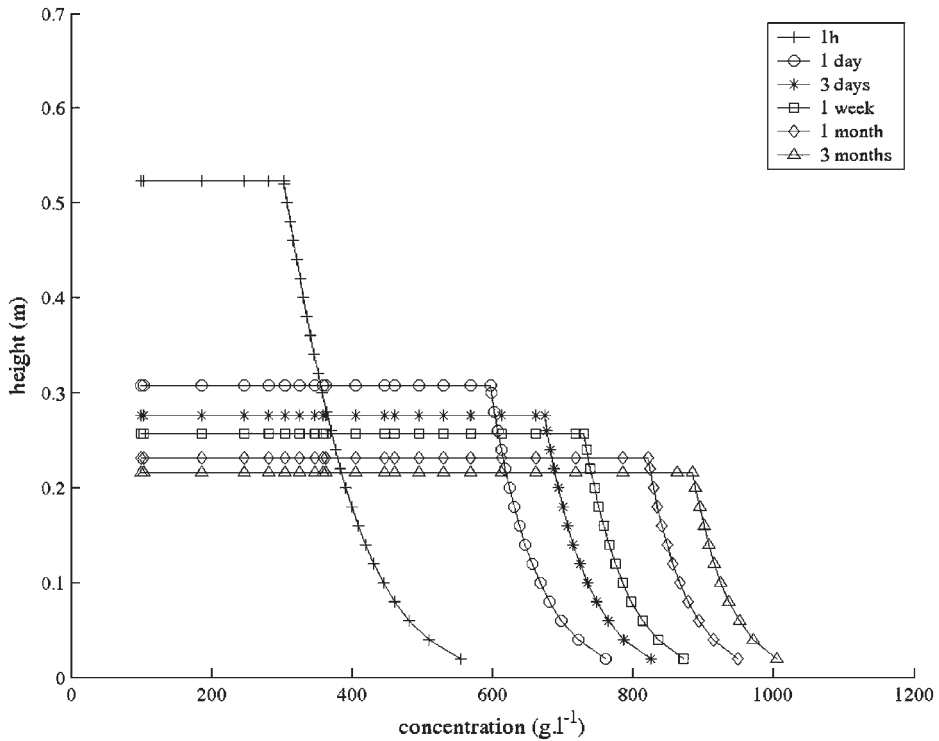


Figure 8. Simulated compaction of an initially 1 m tall settling tube of a sediment–water mixture of 100 g/L.

and concentration of a 1 m tall settling column of a mud–water mixture with initial concentration of 100 g/L. These curves show, for instance, that the sediment height is one third of its initial value after 1 day and that the concentration exceeds 800 g/L after 10 days, which conforms to Migniot’s experimental results.

No morphodynamic coupling is taken into account in these simulations: the sediment compartment is treated independently of the water column. It acts as a source and sink of sediments, and erosion or deposition does not affect the bathymetry.

Results are shown in Fig. 9. After 1 year, the sediment is eroded from the eastern part of the domain, where a system of very dynamic sandy channels is observed in nature: the tidal currents do not allow muddy deposits to remain in that area, except on the highest tidal flats, which are only reached during spring tides. In the central part of the bay, south of the mussel farms, high tidal velocities have eroded the sediment of the tidal flat, whereas a thicker ‘belt’ of deposits is observed on the highest part of the flat, as well as in the western part of the bay, throughout the entire flat (around point D). This area is known to be the muddiest in the bay (also because it is sheltered from waves).

The main effect of the mussel farms is that they cause major erosion at their edges (Fig. 10), where velocity increases are the largest. Depositional areas are seen, in contrast, on the onshore side of these edges, as well as offshore the central farms. The depositional trend of the western part of the bay is reinforced.

1b  
2  
3  
4  
5  
6  
7  
8  
9  
10  
11  
12  
13  
14  
15  
16  
17  
18  
19  
20  
21  
22  
23  
24  
25  
26  
27  
28  
29  
30  
31  
32  
33  
34  
35  
36  
37  
38  
39  
40  
41  
42  
43  
44  
45  
46

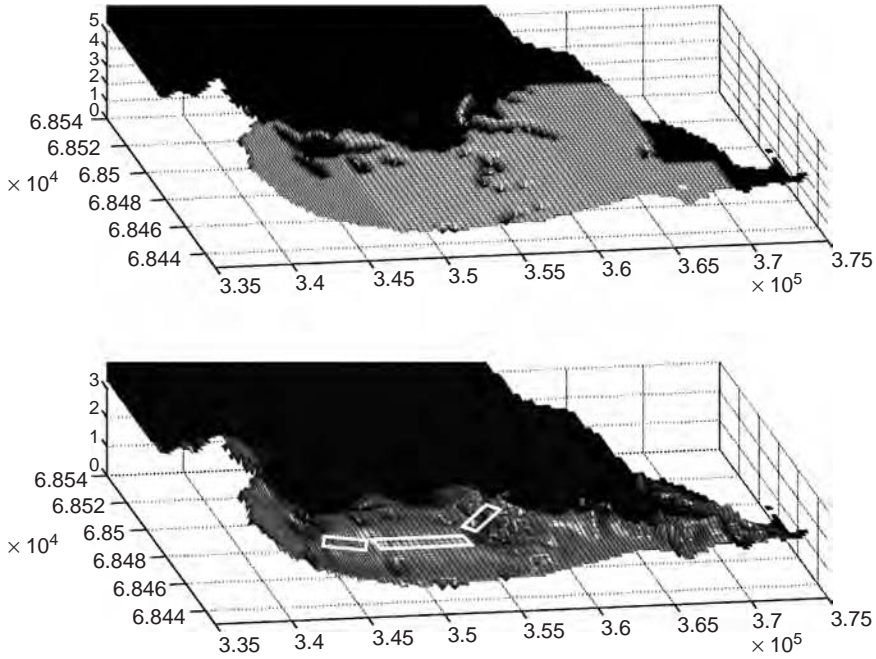


Figure 9. Initial uniform sediment thickness (top) and thickness after 1 year with mussel farms (bottom).

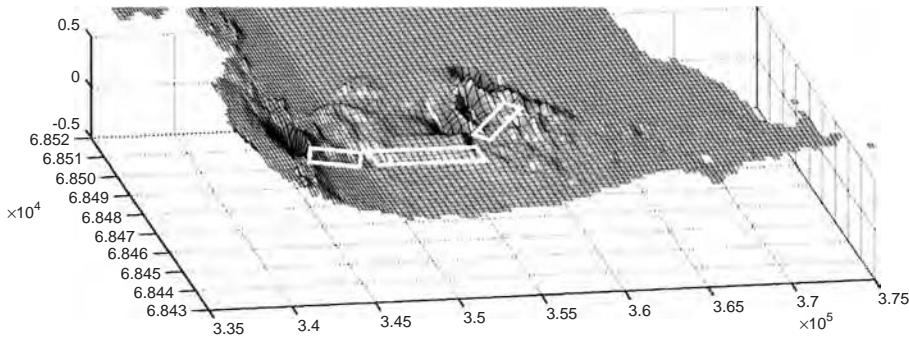


Figure 10. Difference in sediment thickness between the situation with and without farms after 1 year of simulation.

Time evolution of sediment thickness and concentrations of suspended sediment are depicted at four points (Fig. 11; see Fig. 6 for the location of the points). These time series represent results every 2 h. Results are shown 6 months after the beginning of the run (where a uniform layer of 0.3 m of deposits was prescribed). Point A is located at the western tip of the farms, where the largest increases in tidal velocities are computed. While this area is shown to be very stable without farms, continuous erosion is predicted when farms are present. The high velocities computed at this location are actually not compatible with a muddy sedimentary coverage. Offshore the farms, point B behaves in similar way with

1b  
2  
3  
4  
5  
6  
7  
8  
9  
10  
11  
12  
13  
14  
15  
16  
17  
18  
19  
20  
21  
22  
23  
24  
25  
26  
27  
28  
29  
30  
31  
32  
33  
34  
35  
36  
37  
38  
39  
40  
41  
42  
43  
44  
45  
46

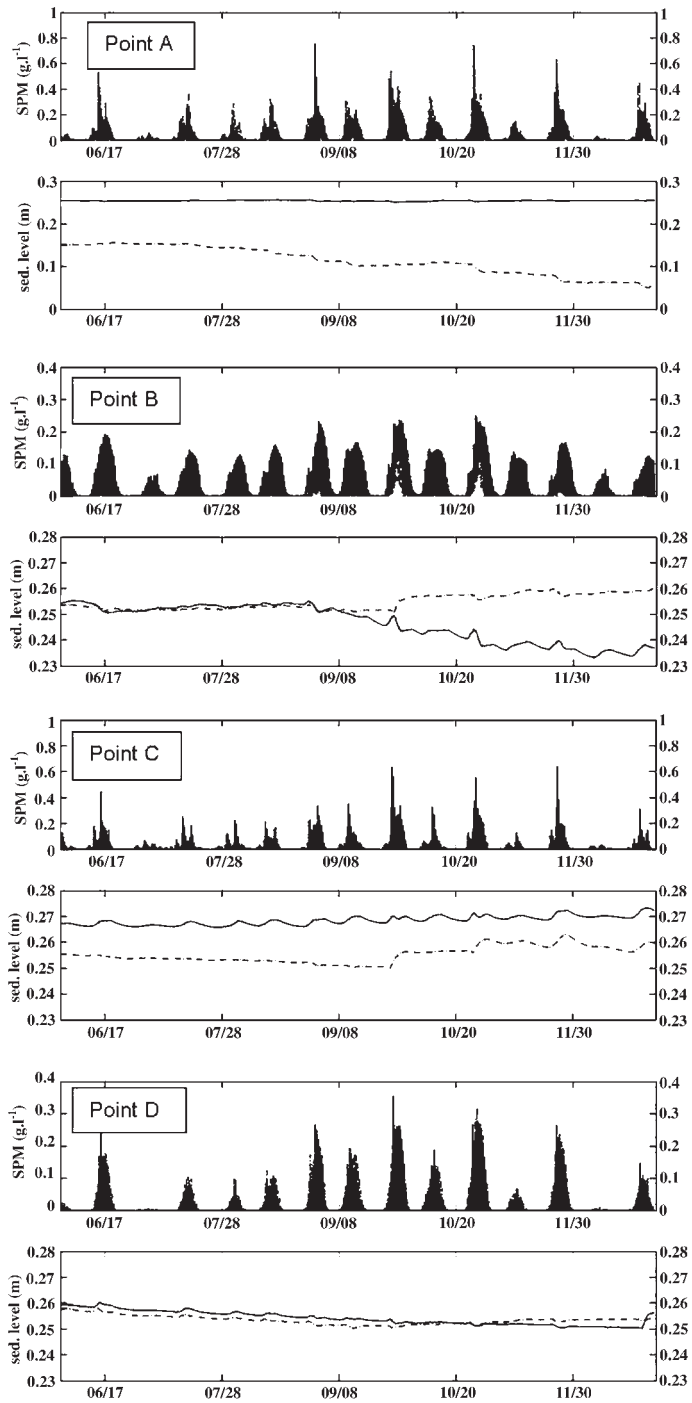


Figure 11. Evolution of the suspended concentration and the sediment level for points A, B, C and D (see Fig. 6 for location) over 6 months. Solid line: situation without farms; dashed line: situation with farms.



1b or without the farms, except during large spring tides, which are responsible for erosion  
2 without farms, and deposition with the farms. The same trend is observed within the farms.  
3 At point C, the farms initially induce excess erosion. However, after a few months, this  
4 trend stabilizes, and no significant difference is seen with or without the farms. Suspended  
5 concentrations are of the correct order of magnitude, with flood and ebb peaks of the order  
6 of 0.2–1 g/L depending on the area. The influence of the farms on the suspended concen-  
7 tration pattern is not significant.

8  
9

## 10 **6. CONCLUSION**

11

12 The analysis of the tide and waves contributions in the Mont Saint Michel Bay suggests two  
13 main results: (1) the tidal dynamics may account to a large extent to the sediment distribu-  
14 tion in the bay; (2) waves being the most efficient factor for resuspension, the concentration  
15 of suspended sediments decreases from east to west, as wave effects are dampened by the  
16 sheltering effect of the cape located at the north-west end of the bay. As a consequence, con-  
17 centrations of suspended matter are well correlated twith the occurrence of waves in the  
18 central part of the bay, while tidal effects become dominant in the east.

19

20 Using an initial condition based on uniform mud coverage of Mont Saint Michel Bay,  
21 the main features of the observed mud distribution are reproduced, i.e. deposition of mud  
22 on the upper part of the intertidal profile and in the western part of the bay and no deposits  
23 in the eastern channels. The thinner deposits predicted in the middle part of the intertidal  
24 profile correspond to areas actually covered by muddy sands. The presence of mussel  
25 farms was shown to induce erosion by their edges. The amount of predicted erosion seems  
26 to be excessive, since it did not allow muddy deposits to remain near the edges of the  
27 farms, which is not observed in the field. The amount of overall added friction in the farms  
28 must therefore be overestimated, which induces an overestimation of the velocity increase  
29 as well. The farms were also shown to encourage sedimentation within the farms them-  
30 selves, as well as onshore or offshore the farms depending on the local dynamics.

31

32 These results need to be interpreted keeping in mind the main approximations that were  
33 made for the numerical modelling:

34

35 1. Waves were not taken into account. Wave measurements as well as preliminary  
36 computations of wave propagation show that wave-induced bottom shear stress in  
37 Mont Saint Michel Bay can be as high as 10 times the maximum tide-induced shear  
38 stress. While the overall sediment distribution is well explained by the tidal dynamics,  
39 the proper simulation of suspended matter concentrations requires waves to be taken  
40 into account.

41

42 2. The muddy fraction was only taken into account. As a response to a longshore and  
43 cross-shore variability of the bottom shear stress, the sediment coverage in the bay is  
44 very much dependent on the location. This environment typically requires the use of  
45 a mixed grain size model, which is an option that was not included for these runs.  
46 This is particularly true in areas where fine sands are mixed with cohesive sediments:  
the single mud fraction will predict a bare bottom where mud may, in reality, be  
trapped by sand. The parameterization of erosion thresholds and erosion fluxes of  
natural sediments in the bay is also under investigation (Le Hir et al., 2005).

- 1b 3. Mussel farms were represented in the model through a local increase in the friction  
 2 coefficient, which was probably overestimated using values from the literature.  
 3 Measurements of tidal velocities around the farms need to be carried out in order to  
 4 validate the magnitude of the velocity changes due to these structures.  
 5  
 6


7 **REFERENCES**

8  
 9 Bahé, S. (2003). Conchyliculture et dynamique morpho-sédimentaire en Baie du Mont Saint-Michel: Mise en  
 10 place d'une base de données géographiues. *Master's Thesis*, EPHE, Laboratoire de Géomorphologie et  
 11 Environnement Littoral, pp. 161.  
 12 Bonnot-Courtois, C., Caline, B., L'Homer, A. and Le Vot, M. (2002). Baie du Mont Saint-Michel et Estuaire  
 13 de la Rance: Environnements sédimentaires, aménagements et évolution récente. *Editions TotalFinaElf*,  
 14 *Mémoire n° 26*, pp. 256.  
 15 Ehrhold, A. (1999). Dynamique de comblement d'un bassin sédimentaire soumis à un régime mégatidal: Exemple  
 16 de la Baie du Mont Saint Michel. *Thesis*, Université de Caen, France, pp. 294. **AQ4**  
 17 Le Hir, P., Cann, P., Waeles, B. and Bassoullet, P. (2005). Erodability of natural sediments: Towards an erosion  
 18 law for sand/mud mixtures from laboratory and field erosion tests. *Proceedings of the INTERCOH2005*  
 19 *Conference*, Saga, Japan (this volume). **AQ5**  
 20 Le Roy, R. and Simon, B.(2003). Réalisation et validation d'un modèle de marée en Manche et dans le Golfe de  
 21 Gascogne; Application à la réalisation d'un nouveau programme de réduction des sondages bathymétriques,  
 22 Rapport d'études SHOM 002/03.  
 23 Migniot, C.(1998). Rétablissement du caractère maritime du Mont Saint Michel, Synthèse des connaissances  
 24 hydro-sédimentaires de la Baie, Direction Départementale de l'uipelement de la Manche, Report, 111 pp.  
 25 SEAMER (2000). Etude d'impact de la restructuration conchylicoles en Baie du Mont Saint Michel, Etude  
 26 courantologique et sédimentologique, Rapport SRC Bretagne Nord, pp. 41.  
 27 SOGREA (1986). Amélioration de la mytiliculture dans la Baie de l'Aiguillon, Rapport LCHF.  
 28 Waeles, B., Le Hir, P., Lesueur, P., Delsinne, N.(2005). Modelling sand/mud transport and morphodynamics in  
 29 the Seine river mouth (France): An attempt by using a process-based approach, (in press). **AQ6**  
 30  
 31  
 32  
 33  
 34  
 35  
 36  
 37  
 38  
 39  
 40  
 41  
 42  
 43  
 44  
 45  
 46

---

**AUTHOR QUERY FORM**


---

 <small>ELSEVIER</small>	<b>Book :</b> SE-KUSUDA	<b>Please e-mail or fax your responses and any corrections to:</b> <b>E-mail:</b> <b>Fax:</b>
	<b>Chapter :</b> 29	

Dear Author,

During the preparation of your manuscript for typesetting, some questions may have arisen. These are listed below. Please check your typeset proof carefully and mark any corrections in the margin of the proof or compile them as a separate list\*.

**Disk use**

Sometimes we are unable to process the electronic file of your article and/or artwork. If this is the case, we have proceeded by:

Scanning (parts of) your article     Rekeying (parts of) your article     Scanning the artwork

*Uncited references*: This section comprises references that occur in the reference list but not in the body of the text. Please position each reference in the text or delete it. Any reference not dealt with will be retained in this section.

**Queries and / or remarks**

Location in Article	Query / remark	Response
AQ1	Au: The sentence seems to end abruptly. Please check whether the insertion of the phrase "feed the bay" brings out the intended meaning.	
AQ2	Au: The years for reference citations Le Hir (2000), Le Hir (2001) and Le Hir (2006) have been changed to 2005 to match the reference list. Please check and confirm.	
AQ3	Au: Please provide the complete bibliographic detail for the reference citation Jestin et al. (1994) so that it can be included in the reference list.	
AQ4	Au: Please confirm whether this is a master's thesis or a doctoral thesis.	
AQ5	Au: Please check whether this reference citation refers to Chapter 11 of this volume. If so, does the chapter title need to be changed?	
AQ6	Au: Please provide the complete details for the reference Waeles et al. (2005).	
AQ7	Au: Has permission been obtained for Fig. 4? If so, please provide the permission line.	

Thank you for your assistance